

Spatial filter masks optimization using genetic algorithm and modeling dynamic behavior of sEMG and finger force signals

ANISH SEBASTIAN, PARMOD KUMAR, MARCO P. SCHOEN

Abstract – Electromyography (EMG) signals are widely used for clinical and biomedical applications. One of the rapidly advancing fields of application of EMG is in the control of smart prosthetic devices for rehabilitation purposes. This paper presents the investigation of the use of System Identification (SI) for modeling sEMG-Finger force relation in the pursuit of improving the control of a smart prosthetic hand. Finger force and sEMG data are generated by having the subject perform a number of random motions of the ring finger to simulate various force levels. Post-processing of the sEMG signal is performed using spatial filtering. The linear and nonlinear spatial filters are compared based on the ‘kurtosis’ improvements and also based on the fit values of the models obtained using system identification, in particular the Hammerstein-Wiener models. The results of the modeling using linear spatial filters were found to be in the region of 30-45%, some of these linear spatial filter masks were selected randomly to investigate if there is any improvement in modeling the sEMG-force relation. The spatial filter masks are optimized using a Genetic Algorithm (GA) for two conditions; constrained and unconstrained. The model fit values of the identified models are used as the cost function in the GA optimization scheme. The results are compared to the reported filter mask values in the literature. The unconstrained GA based filter mask values and in some instances the constrained GA based mask values perform better than the filter masks reported in literature in 24 out of the 26 cases tested.

Keywords— Spatial Filtering, System Identification, Surface Electromyogram, Sensor Array, Genetic Algorithm, Hammerstein-Wiener Modeling.

I. INTRODUCTION

IN the United States there are approximately 1.7 million people living with limb loss [1]. It is estimated that one out of every 200 people in the U.S. has had an amputation [2]. An ideal prosthetic hand has to be dexterous; easy to manufacture, must use little power and at the same time, must be of low cost. Building such a prosthetic hand, which can mimic the entire gamut of motions and have the functionality and

dexterity of a human hand exactly, has eluded researchers so far. Most of the hand grasping motions that a prosthetic device would need to perform have been classified by Feix [3]. One of the main strategies used in making a prosthetic hand “user friendly” is to use the electromyogram (EMG) signal to control a prosthetic device. An EMG signal is a small voltage signal (in mV) which is generated by skeletal muscles. EMG signals have a wide range of applications in the fields of medicine (orthopedic, surgery, functional neurology and gait and posture analysis), rehabilitation (post surgery/accident, neurological rehabilitation, physical therapy and active training therapy), ergonomics (risk prevention, ergonomic design, etc.) and sports science (biomechanics, movement analysis, athlete strength training and sports rehabilitation). EMG is measured using fine wire intramuscular electrodes, needle electrodes, or on the surface of the skin over the motor point using surface electrodes. Surface electrodes are quick and easy to apply, do not need medical supervision, cause minimal discomfort and are generally suited for superficial muscles. Needle electrodes on the other hand require trained medical professionals for appropriate placement within the muscle. The study of EMG signals, whether they are recorded using needle sensors or by placing electrodes on the surface of the skin, can provide a window into the fascinating world of how the motors of our body work seamlessly to meet the rigorous demands we place on them. The first investigator of EMG signals is considered to be H. Piper in 1912, [4]. Since then, there have been significant advances in the field of EMG signaling. Now, we have a much better understanding of what information can be derived from EMG signals and the various applications they could be used for. Needle EMG sensors are considered more accurate than surface EMG methods, as they can detect Motor Unit Action Potentials (MUAPs) in a very small volume, as small as a tip of a needle. Nonetheless, surface EMG signals also, are used in a large number of applications. One must be careful though, when drawing “conclusions” using surface EMG signals, [5].

Surface EMG signals have a variety of clinical and engineering applications. Few of the clinical applications include a) kinesiologic analysis of movement disorders, b) differentiating types of tremors, myoclonus, and dystonia, c) for evaluating gait and posture disturbances, and for evaluating psychophysical measures of reaction and movement time, [6]. Engineering applications include a)

Manuscript received July 5, 2011. The research was sponsored by the US Department of Defense; under the award number W81XWH-10-1-0128 awarded and administered by the U.S. Army Medical Research Acquisition Activity, 820 Chandler Street, Fort Detrick MD 21702-5014.

Anish Sebastian is a PhD student with the Idaho State University Pocatello, Idaho 83201 USA (e-mail: sebaanis@isu.edu).

Parmod Kumar is a PhD student with the Idaho State University Pocatello, Idaho 83201 USA (e-mail: kumaparm@isu.edu)

Marco P. Schoen, Professor, Department of Mechanical Engineering, Colonial Hall 22 Stop 8060 (208) 282-4377 (e-mail: schomarc@isu.edu)

interpretation of neural control signals for research, [7], b) extraction of command signal for control of prosthetic or robotic devices, [8-10] to name a few.

This paper deals with surface electromyogram signals (sEMG). In the past, multiple methods have been investigated for extracting useful information from EMG signals. Some of these methods include employing low-pass or band-pass filtering; others have also used notch filtering to remove power line noise, [11]. Whitening filters can increase the quality of the amplitude estimates of the sEMG signals, [12]. Other methods include Markov models, [13] and fuzzy logic control, [14] – for classification of EMG, and wavelet processing, [15]. Currently, the accepted standardized method on how EMG signals must be recorded and analyzed is set by the International Society of Electromyography and Kinesiology (ISEK) [16].

The EMG signal is a complicated signal, which is controlled by the nervous system and is dependent on the anatomical and physiological properties of muscles. EMG signal acquires noise while traveling through different tissues. Moreover, the EMG detector, particularly surface electrodes collects signals from different motor units simultaneously which may have been generated through the interaction of

different motor unit signals. sEMG signals are influenced by multiple factors, some of which are; a) shape of the volume conductor, b) the thickness of the subcutaneous tissue layers, c) tissue inhomogeneities, d) distribution of the motor unit territories in the muscle, e) size of the motor unit territories, f) distribution and the number of fibers in the motor unit territory, g) length of the fibers, h) spread of the endplates and tendon junctions within the motor units, and i) spread of the innervations zones and tendon regions among motor units. The type of detection system used also plays an important part in influencing the sEMG measurements. Some of the factors which need to be taken into account, with the detection systems, are a) skin electrode contact (impedance, noise), b) spatial filtering for signal detection, c) inter-electrode distance, d) electrode size and shape, and e) inclination of the detection system relative to the muscle fiber orientation, [17]. Some of the processing methods implemented for EMG processing have been mentioned in [18-22]. Fig. 1 shows the locations where surface EMG electrodes might be placed in the vicinity of a muscle and the underlying anatomy of a muscle.

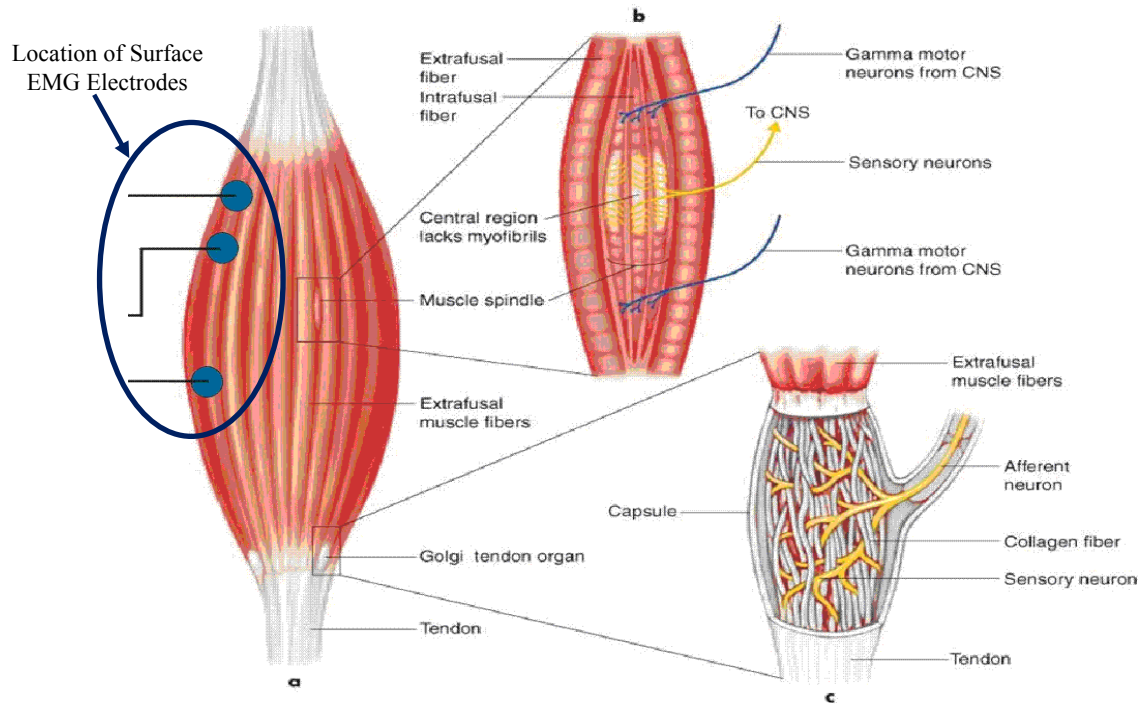


Fig. 1 Muscle anatomy & surface electrodes placement [23]

II. PROBLEM FORMULATION

Measurement of a surface EMG signal, along with an actual recorded sEMG signal is shown in Fig. 2 (a). This EMG signal was obtained from a healthy male subject. The subject had performed squeezing of a stress ball with a force sensitive resistor (FSR) mounted on it. The change in the resistance of the FSR is correlated to the various force level that the subject

could generate. Fig. 2 (b) shows the sEMG plot and the corresponding change in force for one of the experiments performed. As can be seen the sEMG signal is very noisy, it must have been affected by any of the factors that are mentioned in the previous section. Another important factor that influences sEMG signals is cross-talk from the

neighboring motor units of the muscle. All these factors modify the underlying signal for a given contraction and relaxation of the subject's muscle. Many previous works make different assumptions while modeling the sEMG-force relation; like for example, in the simplest form assuming a linear relation between sEMG & force, developing transfer functions of the hand without including the different factors influencing the sEMG signal or using the root-mean-squared (RMS) value of the sEMG signal in order to formulate simplified models.

In reality it is impossible to account for all the factors influencing the sEMG signal. However, by making some of the assumptions mentioned earlier, one might end up with a

deficient model relating the sEMG-force data. The underlying dynamics of the sEMG signal may be lost in the process of oversimplification. In order to avoid some of these pitfalls our approach is to assume a black-box model to deduce a suitable relation or model structure for the two signals. Here, the modeling of the sEMG-finger force relation is not based on root-mean-square, or average values of the sEMG signal, hence, we facilitate the capture of the dynamical changes in the force levels. Our approach of using Hammerstein-Wiener models has been found to be of merit in our previous studies [24, 25] and have yielded satisfactory fits.

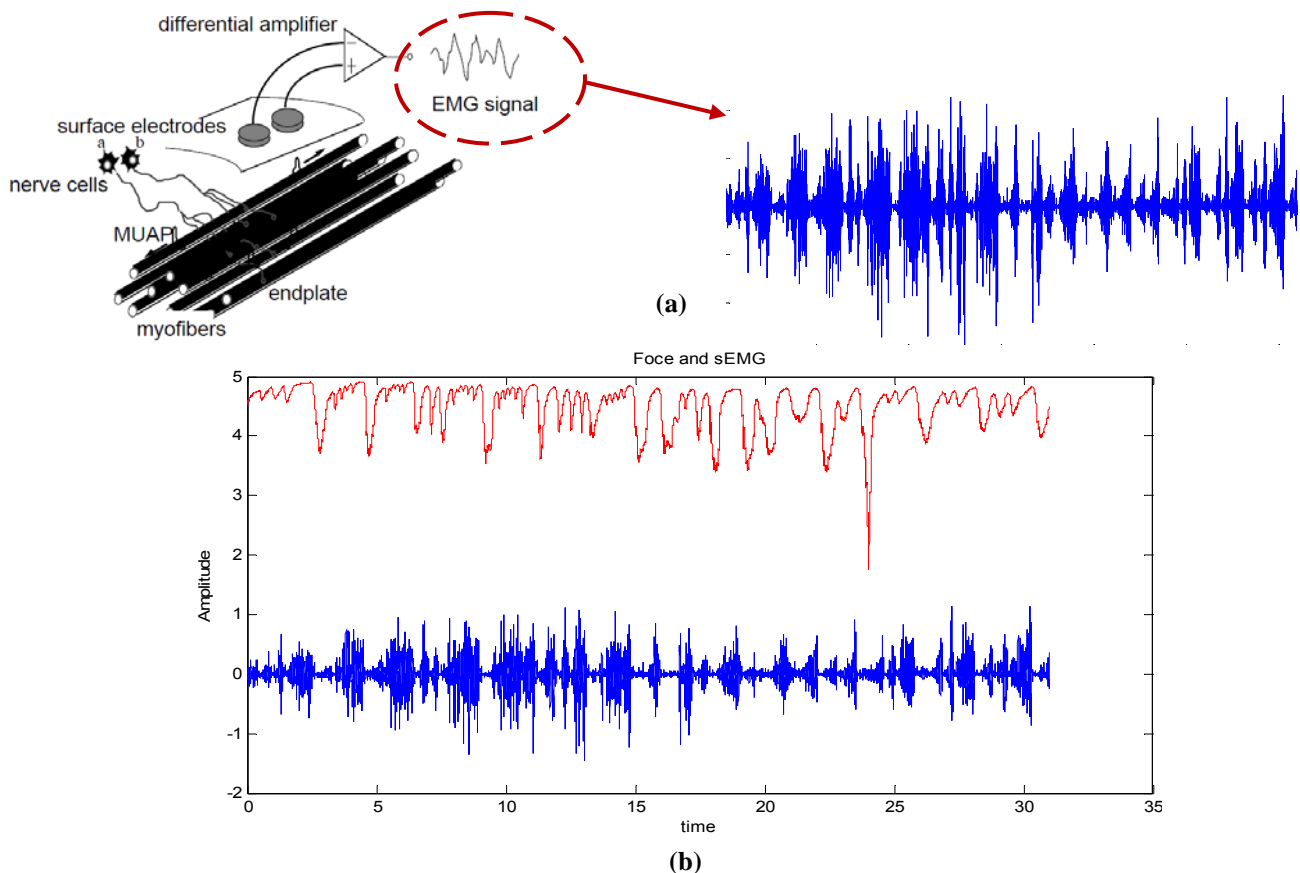


Fig. 2 (a) Measurement of sEMG & actual sEMG from test subject, (b) Force and corresponding sEMG

III. PROBLEM SOLUTION

The data collected is from a nine (3x3) sensor array and rather than analyzing the data only at the motor unit, we considered using spatial filters. Spatial filtering is a very attractive choice as it can be used to either amplify the signal at the motor unit or extract useful information from the entire grid. "Spatial filtering" is broadly defined as a method which computes spatial density estimates for events that have been observed at individual locations. These filters are used when there is no a priori curve to fit to a data series. Instead, it relies on nearby or adjacent, values to estimate the value at a given

point. The most common spatial filters are the low-pass and high-pass spatial filters. These are focal functions whose operation is determined by a kernel or neighborhood of $N \times N$ cells around each pixel or grid position [26]. Grid cells "covered" by a kernel are multiplied by the matching kernel entry and then the weighted average is calculated and assigned as the value for the central cell, G . For example, an asymmetric 3x3 kernel may look like the one shown in Equation (1), or any combination of the weights. Typically a , b are positive integers. If $a=b=1$, then the kernel provides a simple smoothing or averaging operation. Filters of this type

are sometimes referred to as low-pass filters.

$$\text{Symmetric Kernel} = \begin{bmatrix} a & a & a \\ a & b & a \\ a & a & a \end{bmatrix}. \quad (1)$$

The filtered grid value 'G' of an $m=N \times N$ kernel matrix, with C_i set of coefficients and P_i - set of source grid values, is calculated as;

$$G = \frac{\sum_{i=1}^m C_i P_i}{\sum_{i=1}^m C_i} + B. \quad (2)$$

where, B is often set to 0. B is a bias term to increase or decrease the resulting value of 'G'. This kernel is also sometimes referred to as the 'filter mask'. The linear spatial filters tested in this paper are; 1) Longitudinal Single Differential (LSD), 2) Transverse Single Differential (TSD), 3) Longitudinal Double Differential (LDD), 4) Transverse Double Differential (TDD), 5) Normal Double Differential (NDD), 6) Inverse Binomial (IB2) and 7) Inverse Rectangular (IR) Filter. The mask of these filters and the corresponding resultant equations on application of the mask to the grid data obtained from the sEMG array arrangement are given below.

EMG Array Information, [Spatial Filter Mask](#)

$$\text{LSD} = \begin{bmatrix} sEMG7 & sEMG5 & sEMG6 \\ 0 & 0 & 0 \\ sEMG2 & sEMG1 & sEMG3 \\ -1 & 1 & 0 \\ sEMG8 & sEMG4 & sEMG9 \\ 0 & 0 & 0 \end{bmatrix}$$

Result Equation: $-sEMG2 + sEMG1$

$$\text{TSD} = \begin{bmatrix} 0 & -1 & 0 \\ 0 & 1 & 0 \\ 0 & 0 & 0 \end{bmatrix}, \quad \text{LDD} = \begin{bmatrix} 0 & 0 & 0 \\ -1 & 2 & -1 \\ 0 & 0 & 0 \end{bmatrix}, \quad \text{TDD} = \begin{bmatrix} 0 & -1 & 0 \\ 0 & 2 & 0 \\ 0 & -1 & 0 \end{bmatrix}$$

LSD Equation = $sEMG1 - sEMG2$; TSD Equation = $sEMG1 - sEMG5$; we can similarly deduce the equations for the other spatial filters.

$$\text{NDD} = \begin{bmatrix} 0 & -1 & 0 \\ -1 & 4 & -1 \\ 0 & -1 & 0 \end{bmatrix}, \quad \text{IB2} = \begin{bmatrix} -1 & -2 & -1 \\ -2 & 12 & -2 \\ -1 & -2 & -1 \end{bmatrix}, \quad \text{IR} = \begin{bmatrix} -1 & -1 & -1 \\ -1 & 8 & -1 \\ -1 & -1 & -1 \end{bmatrix}$$

In this paper, some nonlinear spatial filters have also been discussed, these have been reported in the literature [27], these are 1) 1-D Nonlinear Transverse spatial filter (NLT), 2) 1-D Nonlinear Longitudinal spatial filter (NLL), 3) 2-D Nonlinear spatial filter in Two- Orthogonal Directions (NLTOD) and 4) Nonlinear spatial filter in All Four possible Directions (NLAFD). The Nonlinear Spatial Filters use the Teager-

Kaiser Energy (TKE) Operator [28]. This technique is a threshold 'energy' based approach where outliers are first detected and then replaced by their estimated values. General Form of Nonlinear Spatial Filter using the Teager-Kaiser (TKE) operator is given in equation (4), where $x(n)$ denotes the location of the sensor in the grid;

$$\Psi[x(n)] = x^2(n) - x(n+1)x(n-1). \quad (4)$$

a) 1-D Nonlinear Transverse Spatial Filter (NLT); equation (5)

$$\Psi_{d,m}[x(m,n)] = x^2(m,n) - x(m-1,n)x(m+1,n). \quad (5)$$

where, d , is the subscript for the dimension, for the 1-D filters it is 1 and m denotes the longitudinal direction i.e. along the muscle fiber.

b) 1-D Nonlinear Longitudinal Spatial Filter (NLL); equation (6)

$$\Psi_{d,n}[x(m,n)] = x^2(m,n) - x(m,n-1)x(m,n+1). \quad (6)$$

n denotes the transverse direction i.e. perpendicular to the muscle fiber.

c) Nonlinear Spatial Filter in Two Orthogonal Directions (NLTOD); equation (7)

$$\begin{aligned} \Psi_{d,2}[x(m,n)] &= \Psi_{d,2m}[x(m,n)] + \Psi_{d,n}[x(m,n)] \\ &= 2x^2(m,n) - x(m-1,n)x(m+1,n) - x(m,n-1)x(m,n+1). \end{aligned} \quad (7)$$

d) Nonlinear Spatial Filter in all Four Directions (NLAFD); equation (8)

$$\begin{aligned} \Psi_{d,4}[x(m,n)] &= 4x^2(m,n) - x(m-1,n)x(m+1,n) \\ &\quad - x(m,n-1)x(m,n+1) - x(m-1,n+1)x(m+1,n-1) \\ &\quad - x(m-1,n-1)x(m+1,n+1). \end{aligned} \quad (8)$$

The experiments were carried out on a healthy male subject. The ring finger motor point was located using a muscle stimulator, manufactured by Rich-Mar Corporation (model number HV 1100). Fig. 3 shows a picture of the Muscle Stimulator used. The EMG detection system used was a Delsys, Bagnoli-16 channel EMG (DS-160, S/N-1116). The sensors used for measuring the surface EMG action potentials were three pronged DE 3.1 differential surface electrodes.



Fig. 3 Muscle stimulator

The material for the contacts of the electrode is 99.9% pure silver, the contacts are 10mm long, 1mm in diameter and spaced 10mm apart. The subjects' skin was prepared, according to the ISEK standards, before the sensors were placed over the motor point. The electrodes were placed along the muscle fibers (Flexor Digitorum Superficialis) for recording surface EMG. The reference electrode was placed on the elbow where there is no sEMG signal. Nine different experiments were conducted and the corresponding sEMG signal was measured simultaneously from all the nine (9) sensors. The force generated by the subject's fingers, for a given motion, was measured using a stress ball with a force sensitive resistor (FSR) mounted on it. Fig. 4 shows the location of the FSR on the stress ball.

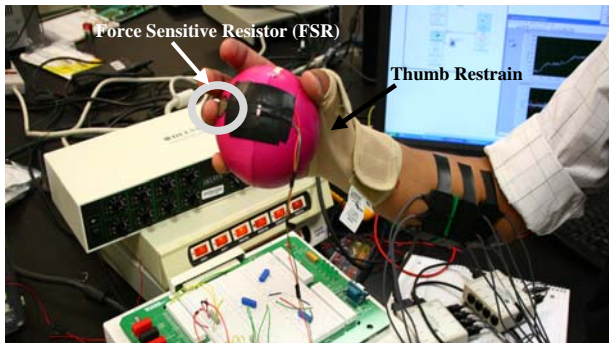


Fig. 4 Force sensitive resistor and thumb restrain

System Identification

System Identification (SI) has its roots in standard statistical techniques, such as least-squares and maximum likelihood methods, for instance. SI helps the user to build mathematical models of a dynamic system based on measured data. This is done by adjusting the parameters within a given model until its output emulates the measured input in some minimum fashion, [29]. System identification is especially useful for modeling systems that cannot be easily represented in terms of first principles or known physical laws. In this case, one can use SI to perform black-box modeling, where the measured data determines the model structure.

Black-box modeling has the following advantages; 1) the structure and the order of the model need not be known, and 2) many model structures can be estimated and compared, and the best among them can be selected to suit the measured data sets. Systems that can be represented using ordinary difference or differential equations can be modeled using grey-box models. Grey-box models have a known mathematical structure and unknown parameters and they have the following advantages over black-box models; 1) Known constraints can be imposed on the model characteristics, 2) there are fewer model parameters to estimate, 3) coupling between parameters can be defined in the model structure, and 4) in the non-linear case the dynamic equations can be specified dynamically.

The most common system identification models in engineering are Auto-Regressive with eXogenous input

(ARX) and Auto-Regressive Moving Average with eXogenous input (ARMAX). The more recent additions to system identification have been black-box models with a non-linear structure such as Artificial Neural Networks, Fuzzy models and so on.

The most basic relationship between the input and the output of a system can be given by a linear difference equation, [30] such as:

$$y(t) + a_1 y(t-1) + \dots + a_n y(t-n) = b_1 u(t-1) + \dots + b_m u(t-m), \quad (9)$$

where, $y(t)$ and $u(t)$ are the input and output of the system at time t respectively, and a_i and b_j are the parameters of the system.

$$\theta = [a_1, \dots, a_n, b_1, \dots, b_m]^T, \quad (10)$$

where, θ is the parametric vector with coefficients a_n and b_m .

$$\varphi(t) = [-y(t-1) \dots -y(t-n) u(t-1) \dots u(t-m)]^T, \quad (11)$$

$$\text{then we can write: } y(t) = \varphi^T(t) \theta, \quad (12)$$

where, $\varphi(t)$ is the regression vector.

Generally, a model structure is a parameterized mapping from past inputs and outputs Z^{t-1} to the space of the model outputs, [31]:

$$\hat{y}(t | \theta) = g(\theta, Z^{t-1}), \quad (13)$$

where, $\hat{y}(t)$ is the predicted output.

In practice most of the systems are nonlinear and the output is a non-linear function of the input variables. However, linear models often sufficiently and accurately describe system dynamics. While modeling a system using grey-box models, the linear and the nonlinear structures can be set using its differential or difference equations. Since linear models are adequate for many situations, it should be tried first to see if the results of the model fit are satisfactory.

It is a possible and a quite common situation where the dynamics of the system can be well described using linear models, but they do not account for any static nonlinearities at the input and/or at the output. This might be the case if the actuators are nonlinear. For example when saturation occurs or when the sensors employed have nonlinear characteristics. A model with a static nonlinearity at the input is called a Hammerstein model. When the nonlinearity is at the output a Wiener model is more appropriate. The combination of the two is then the Hammerstein-Wiener model, [32]. Refer Fig. 5[A] (a) and (b) for Hammerstein and Wiener models respectively. Consider the Hammerstein case where the static nonlinear function $f(\bullet)$ can be parameterized either in terms of physical parameters, such as saturation point and saturation level, or in black-box terms such as spline-function coefficients. This defines $f(\bullet, \eta)$, [31]. If the linear model is given by, the predicted output model will be in the following form:

Equation 14 describes the Hammerstein-Wiener model structure:

$$w(t) = f(g(t)), \quad b(t) = \frac{B_{j,i}(q)}{F_{j,i}(q)} w(t), \quad y(t) = h(x(t)), \quad (14)$$

where, $w(t)$ and $b(t)$ are internal variables, $w(t)$ has the same

dimensions as $u(t)$ - input, and $x(t)$ has the same dimensions as $y(t)$ - output. $g()$ and $h()$ are the input and output non-linearity functions respectively. $B(q)$ and $F(q)$ are regression polynomials. Fig. 5[A] and 5[B] represent the Hammerstein-Wiener models individually and their combination respectively. The model fit values are computed using Equation 15 as follows;

$$fit = 100 * \frac{1 - \|\hat{y} - y\|}{\|y - \hat{y}\|} \quad (15)$$

where, \hat{y} is the estimated output by the model. The linear block is specified using the terms n_b - the number of zeros plus one, n_f - the number of poles and n_k - the delay from the input to the output in terms of the number of samples. The commonly used nonlinear estimators for Hammerstein-Wiener model are, a) Dead Zone, b) Piecewise Linear, c) Saturation, d) Sigmoid Network, and e) Wavelet Network, [32].

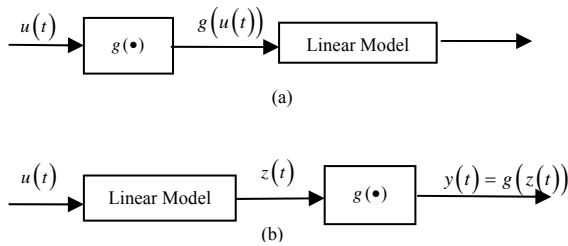


Fig. 5 [A] (a) Hammerstein Model, (b) Wiener Model

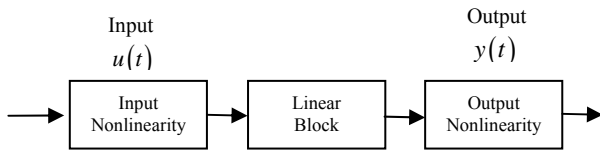


Fig. 5 [B] Hammerstein-Wiener model structure

Genetic Algorithm (GA)

Genetic Algorithm is a class of evolutionary methods for solving both constrained and unconstrained optimization problems that are based on natural selection. This is the same rule that governs biological systems. In GA, the population of individual solutions is modified repeatedly. A solution is given by a set of parameters (genes) and packaged as a chromosome. Each step or iteration the GA selects individuals (chromosomes) in a fashion that may include some randomness, from a given population, as parents, and uses them to produce offspring for the next generation. Over successive iterations or generations, the population evolves and finally reaches an optimal solution. The steps that make

up GA are as follows:

- 1) Generate a random population of 'p' chromosomes – these chromosomes carry information of the population and are confined in the feasible solution space.
- 2) Evaluate the objective or fitness function $f(p)$ for each chromosome.
- 3) Create a new population or offspring from the initial population by using certain rules.

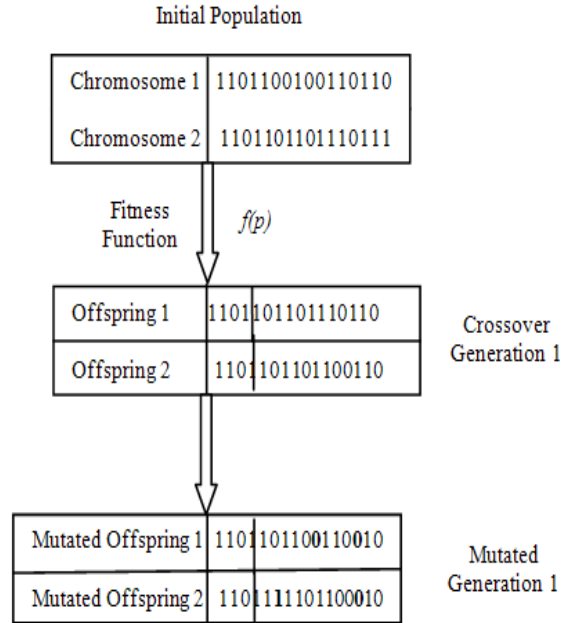


Fig. 6 General steps in a binary genetic algorithm

These rules include a) Selection – selection of two parent chromosomes from the population according to their fitness. b) Crossover – crossover the parents to form new offspring, if no crossover is performed then the offspring is an exact copy of the parents. c) Mutation – involves the changing of a variable in a chromosome or some other change in the original chromosome as defined by the user. d) Acceptance Condition – if offspring satisfies the acceptance condition, include offspring in the new population or else discard. 4) Use the offspring as the parents for the generation of a new population. 5) Continue until the end condition is satisfied. Fig. 6 presents a graphical interpretation of the steps in GA. In this work, GA is used to assist in finding the optimal values of the filter mask for the filtration of the sEMG signal using the various spatial filters. The cost function that the GA tries to minimize, is the model fit obtained from system identification of the sEMG-force data that was collected.

Fig. 7 gives an overview of the method that was followed for this paper.

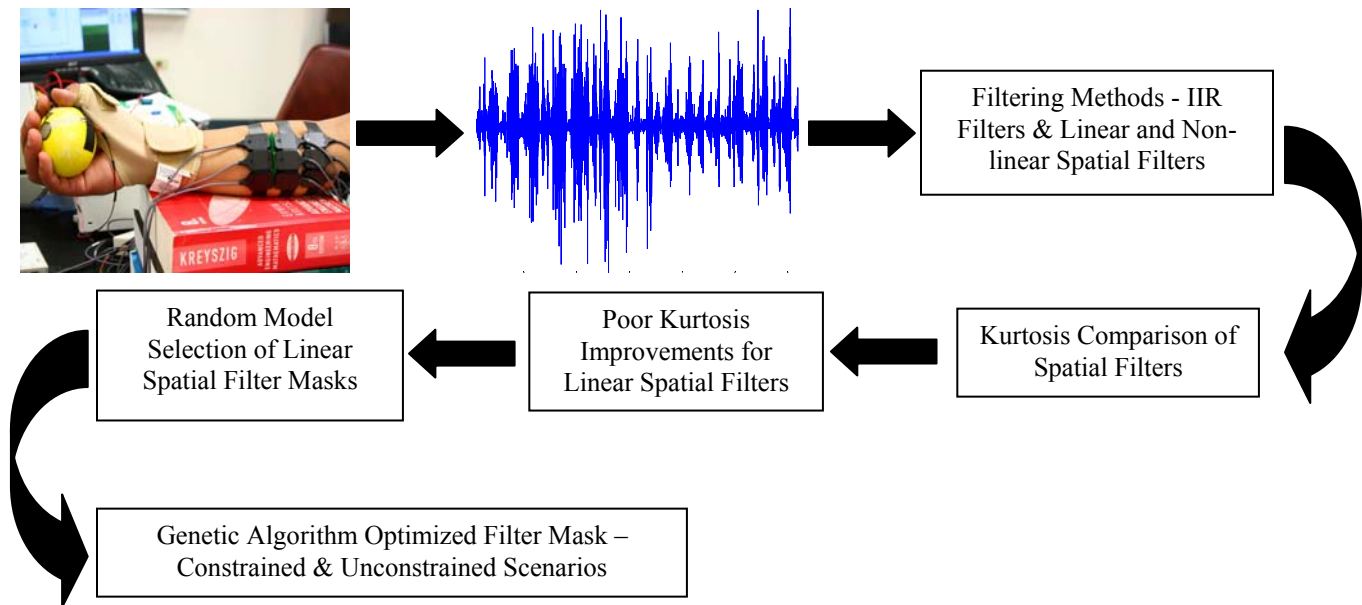


Fig. 7 Overview of the methodology used

IV. SIMULATION RESULTS

The results of spatially filtered data for the linear and the nonlinear spatial filters were first compared based on the “Kurtosis” criteria, [27-28]. ‘Kurtosis’ is a measure of whether the data sets are peaked or flat relative to a normal distribution. That is, data sets with high kurtosis tend to have a distinct peak near the mean, decline rather rapidly, and have heavy tails. Data sets with low kurtosis tend to have a flat top near the mean rather than a sharp peak. A uniform distribution would be the extreme case. The mathematical expression for kurtosis is given in Equation 11.

$$Kurt = \frac{E[x^4] - 3(E[x^2])^2}{E[x^2]^2}. \quad (11)$$

Fig. 8 shows the plot obtained for the various filters based on the kurtosis measure. The y-axis is the kurtosis improvements which is the ratio of the output to the input kurtosis. It is evident from the plot that the NLT, NLL, NLTO and the NLAFD spatial filters performed very well as compared to the linear spatial filters under investigation. The best kurtosis improvements were obtained for experiment 4 \approx 44 for the nonlinear spatial filters. The x-axis in Fig. 5 shows the numbers allotted to the various spatial filters investigated. Based on these results we focused our attention to the linear spatial filter masks for experiment 3, which exhibits poor model fit percentages and also low kurtosis values. This paper does not investigate the reason for the low kurtosis values of the linear spatial filters but only investigates the use of GA to improve the low model fit percentages obtained for experiment 3. The filters were compared based on the model fit values obtained from various Hammerstein-Wiener models.

The Matlab^R code for the Hammerstein-Wiener model is:

$nlhw(ze, [n_b \ n_f \ n_k], \dots, \dots)$. The modeling was carried out by varying n_b - the number of zeros plus one, n_f - the number of poles and n_k - the delay from input and output in terms of the number of samples for the various Hammerstein-Wiener models. In all, 42 models with variations in n_a and n_b were tested while the value of n_k was kept as 1. The total number of models estimated were 7 (filter types) x 4 (time windows) x 42 models per time window = 1,176 models. The time windows used for estimation and validation of the models were called ‘ze’ and ‘zv’ respectively. ‘ze’ contained 8000 sample points and ‘zv’ contained data points shifted by 2000 sample points. For example, if ‘ze’ was a time window between 2-6 seconds i.e. samples 4000-12000, then ‘zv’ was between 3-7 seconds i.e. 6000-14000 samples. These models were computed using the filter masks available in literature. On examining the fit values closely we found them to have large variation from one model order to another. One of the reasons of this could be due to the poor correlation in the estimation and validation data sets, on account of the large variations that were achieved in the force. This paper does not list all these models tested but identifies and reports only the significant results of the analysis. We found that the filters tested performed poorly in the initial time window of 2-7 seconds for experiment 3. Some of the models for this time window were selected and then recomputed using GA to optimize the filter mask with the fitness function being the fit value of an identified model achieved for a given model order.

**Comparison of Spatial Filters
Exp 1 to 9 - With Force (Raw Data)**

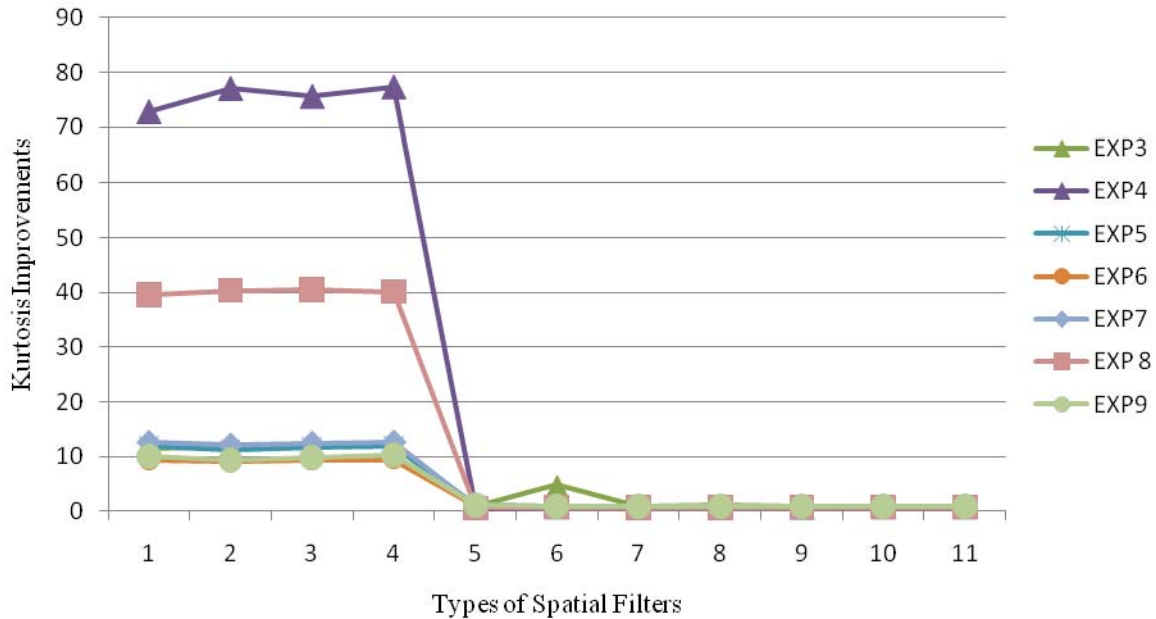


Fig. 8 Kurtosis plots of various filters for exp3 – 9; y-axis numbers are for the various filters tested 1-NLT, 2-NLL, 3-NLTO, 4-NLAFD, 5-LSD, 6-TSD, 7-LDD, 8-TDD, 9-NDD, 10-IB2, and 10- IR

Table 1 shows an example of the fits that were obtained on varying the parameters of the Hammerstein-Wiener model. The highlighted models (and a few other models) were selected randomly to be optimized using GA. We had two scenarios under GA –1) GA Constrained and 2) GA – Unconstrained. The first scenario GA constrained optimized only the mask entry a_{22} (location of the sEMG sensor on the motor unit). The other entries of the filter mask were then

computed from this optimized value. In the second scenario, GA unconstrained we let GA optimize all the entries for various masks. The GA parameters for optimization were as follows: number of iterations: 50; initial population size Generation 0: 96; population size Generation 1: 48; Number of Chromosomes kept for mating: 24; and mutation rate was set to 4%. Figure 9 shows the difference between the two GA scenarios.

Table 1 Example of System Identification Results Using Filter Mask from Literature – Highlighted Models Optimized using GA

| Model Number | n_a | n_b | n_k | LDD | LSD | TDD | TSD | NDD | IB2 | IR |
|--------------|-------|-------|-------|--------|--------|-------|--------|-------|-------|-------|
| m1 | 2 | 3 | 1 | 31.06 | 41.39 | 39.53 | -9.685 | 45.55 | 33.79 | 35.38 |
| m2 | 2 | 4 | 1 | 31.86 | 17.4 | 39.36 | 43.19 | 36.84 | 16.88 | 23.89 |
| m3 | 2 | 5 | 1 | 23.54 | 35.94 | 30.09 | 2.247 | 39.78 | 36.17 | 38.16 |
| m4 | 2 | 6 | 1 | 3.266 | 41.99 | 41.28 | 43.46 | 10.83 | 36.41 | 36.7 |
| m5 | 2 | 7 | 1 | 31.58 | 40.55 | 44.65 | 31.28 | 2.593 | 32.26 | 36.34 |
| m6 | 2 | 8 | 1 | 37.84 | 4.259 | 21.89 | 20.08 | 8.036 | 36.22 | 36.57 |
| m7 | 2 | 9 | 1 | 31.42 | 0.1887 | 35.78 | 28.71 | 38.11 | 35.54 | 35.82 |
| m8 | 3 | 3 | 1 | 36.59 | 40.04 | 36.17 | 12.33 | 4.478 | 41.09 | 35.81 |
| m9 | 3 | 4 | 1 | 20.74 | 40.72 | 31.53 | 36.57 | 29.76 | 37.43 | 38.76 |
| m10 | 3 | 5 | 1 | 39.87 | 11.53 | 39.83 | 30.24 | 39.25 | 35.15 | 37.9 |
| ⋮ | ⋮ | ⋮ | ⋮ | ⋮ | ⋮ | ⋮ | ⋮ | ⋮ | ⋮ | ⋮ |
| m40 | 7 | 7 | 1 | 34.91 | 10.18 | 40.79 | 35.21 | 35.24 | 33.42 | 37.92 |
| m41 | 7 | 8 | 1 | 0.1127 | 36.28 | 39.68 | 40.26 | 20.27 | 35.88 | 24.32 |
| m42 | 7 | 9 | 1 | 36.55 | -0.412 | 25.24 | 31.31 | 35.4 | 34.26 | 39.82 |

Genetic Algorithm

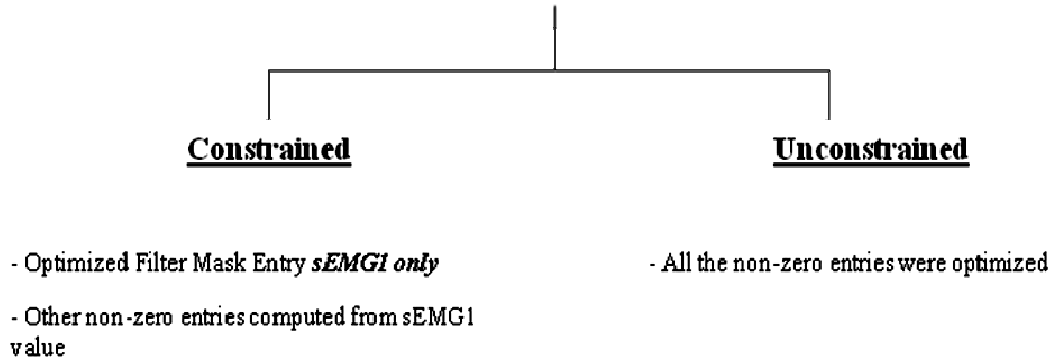


Fig. 9 Two genetic algorithm scenarios tested

Table 2 Results of constrained and unconstrained GA of highlighted models from Table 1

| Longitudinal Double Differential (LDD) | | | |
|--|-----------------|----------------|------------------|
| | Fit % | | |
| | From Literature | GA Constrained | GA Unconstrained |
| m1 | 31.06 | 42.8291 | 61.3475 |
| m6 | 37.84 | 53.3134 | 63.7240 |
| m12 | 35.54 | 44.2513 | 51.7942 |
| m31 | 39.44 | 47.0034 | 60.6489 |

| Longitudinal Single Differential (LSD) | | | |
|--|-----------------|----------------|------------------|
| | Fit % | | |
| | From Literature | GA Constrained | GA Unconstrained |
| m1 | 41.39 | 48.9135 | 57.9136 |
| m4 | 41.99 | 41.5731 | 60.2369 |
| m8 | 40.04 | 40.5924 | 46.3310 |
| m9 | 40.72 | 45.2322 | 45.4538 |

| Transverse Double Differential (TDD) | | | |
|--------------------------------------|-----------------|----------------|------------------|
| | Fit % | | |
| | From Literature | GA Constrained | GA Unconstrained |
| m1 | 39.53 | 41.5297 | 59.8055 |
| m5 | 44.65 | 49.4667 | 68.4191 |
| m10 | 39.83 | 41.307 | 63.8523 |
| m15 | 43.01 | 43.3466 | 56.5113 |

| Transverse Single Differential (TSD) | | | |
|--------------------------------------|-----------------|----------------|------------------|
| | Fit % | | |
| | From Literature | GA Constrained | GA Unconstrained |
| m2 | 43.19 | 44.0017 | 65.9038 |
| m4 | 43.46 | 43.0529 | 58.2755 |
| m11 | 44.24 | 39.7867 | 44.8431 |
| m31 | 29.1 | 43.5787 | 47.6688 |

| Normal Double Differential (NDD) | | | |
|----------------------------------|-----------------|----------------|------------------|
| | Fit % | | |
| | From Literature | GA Constrained | GA Unconstrained |
| m1 | 45.55 | 53.1512 | 57.9496 |
| m3 | 39.87 | 47.1084 | 60.7374 |
| m7 | 38.11 | 51.8065 | 60.5535 |
| m11 | 39.01 | 46.881 | 56.1193 |

| Inverse Binomial 2 (IB2) | | | |
|--------------------------|-----------------|----------------|------------------|
| | Fit % | | |
| | From Literature | GA Constrained | GA Unconstrained |
| m1 | 33.79 | 38.6076 | 58.2365 |
| m3 | 36.17 | 38.9074 | 58.1653 |
| m4 | 36.41 | 38.9957 | 55.5179 |
| m8 | 41.09 | 47.2971 | 55.0537 |

From the results in Table 2 we can see that the optimization of the filter mask using GA worked in almost all the cases chosen. GA without constraints performed significantly better, in most cases, than the filter masks reported in literature and also the mask which we computed using GA, which only optimized the entry (a_{22}) i.e. the weight associated with the sEMG signal at the motor unit. This restriction on GA would

leave the filter mask symmetrical. But looking at the results of the GA, we can conclude that the filter mask need not always be symmetrical for analysis of sEMG, especially for data recorded using an array. All the filter masks, with the individual entries of the masks that were obtained after optimization along with the respective fit values are provided in Table 3.

Table 3 Optimized filter masks for constrained and unconstrained GA

| Linear Spatial Filter Type | Mask in Literature | GA Optimized Spatial Filter Mask - Constrained | GA Optimized Spatial Filter Mask - Unconstrained |
|----------------------------|--|---|--|
| LDD m1 | $\begin{bmatrix} 0 & 0 & 0 \\ -1 & 2 & -1 \\ 0 & 0 & 0 \end{bmatrix}$ Fit 31.06 % | $\begin{bmatrix} 0 & 0 & 0 \\ -6.5 & 13 & -6.5 \\ 0 & 0 & 0 \end{bmatrix}$ Fit 42.8912 % | $\begin{bmatrix} 0 & 0 & 0 \\ -64.2686 & 23.5033 & -20.8633 \\ 0 & 0 & 0 \end{bmatrix}$ Fit 61.3475 % |
| LSD m4 | $\begin{bmatrix} 0 & 0 & 0 \\ -1 & 1 & 0 \\ 0 & 0 & 0 \end{bmatrix}$ Fit 41.99 % | $\begin{bmatrix} 0 & 0 & 0 \\ -2 & 2 & 0 \\ 0 & 0 & 0 \end{bmatrix}$ Fit 41.5731% | $\begin{bmatrix} 0 & 0 & 0 \\ -52.7866 & 54 & 0 \\ 0 & 0 & 0 \end{bmatrix}$ Fit 60.2369 % |
| TDD m5 | $\begin{bmatrix} 0 & -1 & 0 \\ 0 & 2 & 0 \\ 0 & -1 & 0 \end{bmatrix}$ Fit 44.65 % | $\begin{bmatrix} 0 & -27 & 0 \\ 0 & 54 & 0 \\ 0 & -27 & 0 \end{bmatrix}$ Fit 49.4667 % | $\begin{bmatrix} 0 & -41.5561 & 0 \\ 0 & 54.7329 & 0 \\ 0 & -22 & 0 \end{bmatrix}$ Fit 68.4191 % |
| TSD m2 | $\begin{bmatrix} 0 & -1 & 0 \\ 0 & 1 & 0 \\ 0 & 0 & 0 \end{bmatrix}$ Fit 43.19 % | $\begin{bmatrix} 0 & -28.5 & 0 \\ 0 & 57 & 0 \\ 0 & 0 & 0 \end{bmatrix}$ Fit 44.0017 % | $\begin{bmatrix} 0 & -74 & 0 \\ 0 & 89.6214 & 0 \\ 0 & 0 & 0 \end{bmatrix}$ Fit 65.9038 % |
| NDD m3 | $\begin{bmatrix} 0 & -1 & 0 \\ -1 & 4 & -1 \\ 0 & -1 & 0 \end{bmatrix}$ Fit 39.87 % | $\begin{bmatrix} 0 & -6.75 & 0 \\ -6.75 & 27 & -6.75 \\ 0 & -6.75 & 0 \end{bmatrix}$ Fit 47.1084 % | $\begin{bmatrix} 0 & -11.5790 & 0 \\ -46.7773 & 36.9276 & -11.8061 \\ 0 & -70.0491 & 0 \end{bmatrix}$ Fit 60.7374 % |
| IB2 m1 | $\begin{bmatrix} -1 & -2 & -1 \\ -2 & 12 & -2 \\ -1 & -2 & -1 \end{bmatrix}$ Fit 33.79 % | $\begin{bmatrix} -0.42 & -0.83 & -0.42 \\ -0.83 & 5 & -0.83 \\ -0.42 & -0.83 & -0.42 \end{bmatrix}$ Fit 38.6076 % | $\begin{bmatrix} -9.3405 & -85.0222 & -53.7102 \\ -95.4633 & 42 & -30.7811 \\ -28.6087 & -8.2511 & -10.0189 \end{bmatrix}$ Fit 58.2365 % |

V. CONCLUSION

The linear spatial filter masks as reported in the literature have poor model fit percentages and poor kurtosis improvements. Though the reason for the low *kurtosis* improvements of the linear spatial filters was not investigated here, we optimized the linear spatial filter masks using GA and compared them based on the model fit values achieved. The selected model structure for characterizing the sEMG and finger force data is a Hammerstein-Wiener model. The fit values did improve significantly in the two GA scenarios – GA with and without constraints. The GA without constraints performed better than

the GA with constrains, which brings into focus the possibility that the sEMG signal distribution over the entire grid cannot be assumed to be symmetrically distributed and that the weights associated with the sEMG signal at various locations need to be modified depending on probably the subject and also based on the experimental design. This is in contrast to the reported filter mask in the literature, which are all symmetric. Almost all the filter masks optimized resulted in a significant improvement over the masks reported in literature.

ACKNOWLEDGEMENT

This work was supported by a grant from the Telemedicine Advanced Technology Research Center (TATRC) of the US Department of Defense. The financial

support is greatly appreciated.

REFERENCES

- [1] Kathryn Ziegler-Graham, et al., "Estimating the Prevalence of Limb Loss in the United States - 2005 to 2050," Archives of Physical Medicine and Rehabilitation 89: 2008, pp. 422-429.
- [2] Patricia F. Adams, et al., "Current Estimates from the National Health Interview Survey, 1996," Vital and Health Statistics 10:200, 1999.
- [3] <http://enr.isu.edu/FacultyWebpages/alba/documents/PROSTHETIC-HAND-REQUIREMENTS.pdf>
- [4] Piper, H., 1912. "Elektrophysiologie Menschlicher Muskeln". Springer Verlag.
- [5] Merletti, R., Parker, A. P., 1st ed., "Electromyography Physiology, Engineering, and Non-Invasive Applications". Chap. 1, pp. xv- xviii.
- [6] Pullman, S. L., Goodin, D. S., Marquinez, A. I., Tabbal, S., Rubin, M., 2000. "Clinical utility of surface EMG". *Neurology*, 55, July, pp. 171-177.
- [7] Merletti, R., Roy, S. H., Kupa, E., Roatta, S., Granata, A., 1999. "Modeling of surface myoelectric signals - part II: model-based signal interpretation". *IEEE Trans Biomed Eng*, 46 (7), July, pp. 821-829
- [8] Meek, S. G., Fetherston, S. J., 1992. "Comparison of signal-to-noise ratio of myoelectric filters for prosthesis control". *J Rehabil Res & Dev*, 29(4), Fall, pp. 9-20.
- [9] Light, C. M., Chappell, P. H., Hudgins, B., Engelhart, K., 2002. "Intelligent multifunction myoelectric control of hand prostheses". *Journal of Medical Engineering & Technology*, 26 (4), pp. 139-146.
- [10] Light, C. M., Chappell, P. H., 2000. "Development of a lightweight and adaptable multiple-axis hand prostheses". *Medical Engineering and Physics*, 22, pp. 679-684.
- [11] Mewett, D. T., Nazeran H., Reynolds, K., J., "Removing power line noise from recorded EMG". Proceedings of the 23rd Annual IEEE/EMBS International Conference, October, 2001, pp. 1-4.
- [12] Clancy, A. E., Farry, A. K., "Whitening of the electromyogram to improve amplitude estimation". *IEEE Transactions on Biomedical Engineering*, 47(6), June 2000, pp. 709-719.
- [13] Chan, D. C. A., Englehart, B. K., "Continuous myoelectric control for powered prostheses using hidden Markov models". *IEEE Transactions on Biomedical Engineering*, 52(1), January 2005, pp. 121-124.
- [14] Chan, H. Y. F., Yang, Y., Lam, F. K., Zhang, Y., Parker, A. P., "Fuzzy EMG classification for Prosthesis control". *IEEE Transactions on Rehabilitation Engineering*, 8(3), September 2000, pp. 305-311.
- [15] Reaz, I. B. M., Hussain, S. M., Yasin, M. F., "Techniques of EMG signal analysis: detection, processing, classification and application". *Biomedical Procedures Online*, 8(1), January 2006, pp. 11-35.
- [16] http://www.isek-online.org/standards_emg.html
- [17] Farina, D., Merletti, R., and Enoka, M. R., "The extraction of neural strategies from the surface EMG". *Journal of Applied Physiology*, 96, 2004, pp. 1486-1495.
- [18] Zeghib, A., Palis, F., Tsenov, G., Shoylev, N., Mladenov, V., 2005. "Fuzzy systems and neural networks methods to identify hand and finger movements using surface EMG signals", ICS'05 Proceedings of the 9th WSEAS International Conference on Systems, Vouliagmeni, Athens, Greece, July 11-13.
- [19] Hu, X., Ren, X., 2006. "Identification of Surface EMG Signals Using Wavelet Packet Entropy", Proceedings of the 6th WSEAS International Conference on Wavelet Analysis & Multirate Systems, Bucharest, Romania, October 16-18, pp. 96-99.
- [20] Zeghib, A., Palis, F., Shoylev, N., Mladenov, V., Mastorakis, N., "Sampling frequency and pass-band frequency effects on Neuromuscular Signals (EMG) Recognition", 2007. Proceedings of the 6th WSEAS International Conference on Signal Processing, Robotics and Automation, Corfu Island, Greece, February 16-19, pp. 107-114.
- [21] P. Kumar, C. Potluri, A. Sebastian, S. Chiu, A. Urfer, D. S. Naidu, and M. P. Schoen, "An Adaptive Multi Sensor Data Fusion with Hybrid Nonlinear ARX and Wiener-Hammerstein Models for Skeletal Muscle Force Estimation," The 14th World Scientific and Engineering Academy and Society (WSEAS) International Conference on Systems, Corfu Island, Greece, July 22-24, 2010.
- [22] P. Kumar, A. Sebastian, C. Potluri, A. Ilyas, M. Anugolu, A. Urfer, and M. P. Schoen, "Adaptive Finger Angle Estimation from sEMG Data with Multiple Linear and Nonlinear Model Data Fusion," The 10th World Scientific and Engineering Academy and Society (WSEAS) International Conference on Dynamical Systems and Control, Iasi, Romania, July 1-3, 2011.
- [23] <http://www.tmsi.com/?id=26>
- [24] Sebastian A., Parmod K., Anugolu M., Schoen P. M., Urfer A., Naidu S. D., "Optimization of Bayesian Filters and Hammerstein-Wiener Models for EMG-Force Signals Using Genetic Algorithm". Proceedings of the ASME 2009 Dynamic Systems and Control Conference DSCC 2009.
- [25] Sebastian A., Parmod K., Schoen P. M., Urfer A., Creelman J., Naidu S. D., "Analysis of EMG-Force relation using System Identification and Hammerstein-Wiener Models". Proceedings of the ASME 2010 Dynamic Systems and Control Conference DSCC 2010.
- [26] <http://www.spatialanalysisonline.com/output/html/Linearspatialfiltering.html>
- [27] P. Zhou, N. L. Suresh, M. Lowery, W. Z. Rymer, "Nonlinear Spatial Filtering of Multichannel Surface Electromyogram Signals During Low Force Contractions", *IEEE Transactions on Biomedical Engineering*, vol. 56, no.7, July 2009, pp. 1871-1879.
- [28] J. F. Kaiser, "On a simple algorithm to calculate the 'energy' of a signal", Proceedings of IEEE ICASSP'90, Albuquerque, New Mexico, April 1990, pp. 381-384.
- [29] Ljung, L., 2nd ed., "System Identification: theory for the user". Prentice Hall Information and System Sciences Series, Chap. 1, pp. 1-8.
- [30] Ljung, L., 2nd ed., "System Identification: theory for the user". Prentice Hall Information and System Sciences Series, Chap. 1, pp. 13.
- [31] Ljung, L., 2nd ed., "System Identification: theory for the user". Prentice Hall Information and System Sciences Series, Chap. 5, pp. 140-145.
- [32] http://www.mathworks.com/access/helpdesk/help/toolbox/ident/index.html?access/helpdesk/help/toolbox/ident/gsbq_ylq6.html

Anish Sebastian received his B.S. degree in Instrumentation Engineering from Dr. D.Y. Patil College of Engineering, India in 2002, his M.S. degree in Measurement & Control Engineering from Idaho State University in 2009, and is currently a Ph.D. candidate in the Engineering & Applied Science Program at Idaho State University.

His research interests include development of a Smart Prosthetic Hand, development active flow control to mitigate stall and improve turbine efficiency, radiation therapy for treatment of active nodes in tumors, system identification and control systems. His current research is funded by the Department of Defense (DoD), Telemedicine and Advanced Technology Research Center (TATRC) titled "Smart Prosthetic Hand". He was awarded this research assistantship in 2007. The research being conducted at Idaho State University is on the analysis of surface electromyogram signals (sEMG) in order to establish a relation between the force generated by the fingers while grasping various objects and performing Activities of Daily Living (ADL). From 2005 to 2007 he was a graduate teaching assistant for various departments under the College of Engineering at Idaho State University. Mr Sebastian has 14 publications in all, to date, in internationally reputed conferences and journals. Mr. Sebastian has also served as a reviewer for various international conferences and journals.

Parmod Kumar received his B.S. degree in Marine Engineering from the Marine Engineering & Research Institute, Kolkata, India in 2002, his M.S. degree in Measurement and Control Engineering from Idaho State University

in 2009, and expecting to get his Ph.D. in Engineering and Applied Science from Idaho State University by December 2011. Mr. Kumar has worked in Merchant Navy as a Certified Marine Engineer Officer for over four and half years. From 2007 to 2009 he was a graduate teaching assistant and from 2009 to till now he is a graduate research assistant at Measurement and Control Engineering Research Center (MCERC). Mr Kumar has a wide scope of research interests and published internationally in reputed conferences and journals. Mr Kumar is reviewer for various international conferences and journals. For more details and the list of publications please see the web link <https://sites.google.com/site/parmodkumarms/Home>

Marco P. Schoen was born in 1965 and received his B.S. degree in Mechanical Engineering from the Swiss College of Engineering in 1989, his M.E. degree in Mechanical Engineering from Widener University in 1993, and his Ph.D. in Engineering Mechanics from Old Dominion University in 1997. From 1997 to 1998 he was a faculty member at Lake Superior State University and from 1998 to 2001 he served as a faculty to the Mechanical Engineering program at Indiana Institute of Technology. Since 2001 he has been with Idaho State University, where he currently serves as professor and chair for the Department of Mechanical Engineering and as associate director for the Measurement and Control Engineering Research Center (MCERC). His research addresses topics in controls and vibration of biomedical and aerospace systems as well as energy related problems. Schoen has been an associate editor for the Journal of Dynamic Systems, Measurement and Control, and a past chair of the Model Identification and Intelligent Systems (MIIS) Technical Committee for the American Society of Mechanical Engineers (ASME).